Journal of Materials Chemistry A

Accepted Manuscript

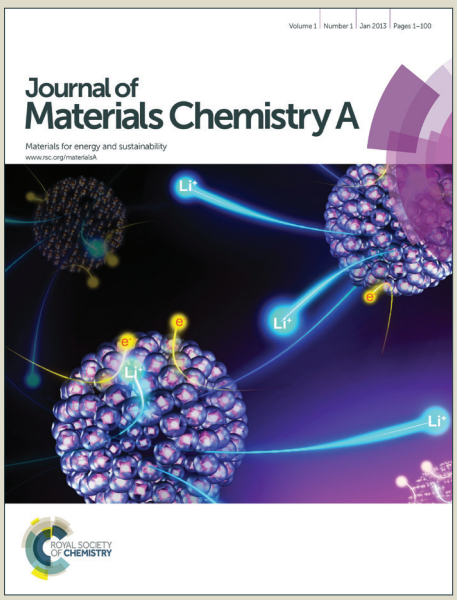

ROYAL SOCIETY OF CHEMISTRY

www.rsc.org/materialsA

Journal Name

RSCPublishing

ARTICLE

Facile synthesis of scalable pore-containing silicon/nitrogen-rich carbon composites from waste contact mass of organosilane industry as anode materials for lithium-ion batteries

Cite this: DOI: 10.1039/xoxxoooooox

Received ooth January 2012,
Accepted ooth January 2012

DOI: 10.1039/xoxxoooooox

www.rsc.org/

Lu Shi,[ab] Weikun Wang,[*b] Anbang Wang,[*b] Keguo Yuan[b] and Yusheng Yang[b]

A series of pore-containing silicon/nitrogen-rich carbon composites are successfully synthesized via a simple method by using the waste contact mass of organosilane industry as the pore-containing silicon source, followed by acid washing to remove the impurities and ball milling to obtain the silicon particles with appropriate particle size. The gelatin is employed as the carbon precursor to gain the nitrogen-rich carbon. The pore-containing silicon/nitrogen-rich carbon composites with different ratios of pore-containing silicon and nitrogen-rich carbon are investigated as anode materials for Li-ion batteries. It is found that the composite displays the best electrochemical performance when the weight ratio of the pore-containing silicon particles and gelatin reaches 1:4. It exhibits a reversible capacity of 748 mA h g^{-1} after 100 cycles at a current density of 100 mA g^{-1} and 457 mA h g^{-1} at 600 mA g^{-1}, much higher than those of commercial graphite.

Introduction

There are growing demands for the next-generation lithium-ion batteries with light weight, high energy density and long cycle life to meet the demands of electric vehicles (EV), hybrid electric vehicles (HEV) and other consumer electronic devices[1,2]. Developing a low-cost electrode material with high energy capacity via a simple method can lead to a significant improvement in the high performance lithium-ion batteries. Among the various anode materials, silicon has attracted considerable attentions due to its much higher theoretical specific capacity (about 4200 mA h g^{-1}) than that of graphite anodes (about 372 mA h g^{-1}) and satisfactory potentials for lithium insertion and extraction(<0.5 V vs. Li/Li^+)[3]. In addition, silicon is the second most abundant element in the earth's crust and is environmentally friendly, indicating its potential to be utilized in large quantities at low cost[4]. Nevertheless, the practical use of silicon has been hindered by its poor performance due to its low intrinsic electric conductivity and the significant volume change during the alloying/dealloying processes of silicon with lithium, which can result in pulverization of the initial particle morphology and causes the loss of electrical contact between active materials and the electrode framework[4,5].

Hence a lot of efforts have been made thus far to overcome these problems, such as preparation of Si/C composites[6-9], dispersion silicon in an active/inactive matrix[10], fabrication of some types of nanostructured silicon materials including silicon nanowires[11-13], silicon nanotubes[14-16], silicon hollow nanospheres[17] and nanoscale thin films[18,19]. Among these strategies, constructing pore-containing Si-based anode materials has been proved effective. Its internal porosity would supply sufficient inner free space to absorb the large volume expansions and ease the internal strain to prevent the particle pulverization and thereby enhance the cycling stability[20-23]. What's more, the dispersion of Si into carbon matrix has triggered particular interest owing to the fact that carbonaceous materials can supply enough space to accommodate the volume expansion/constriction of Si during its alloying/de-alloying processes, and meanwhile it can also maintain good electronic conductivity during charging/discharging cycles. So the pore-containing Si/C composites are synthesized to take advantages of both the pore structure of Si and a highly conductive additive coating of carbonaceous materials on the electrode materials[24-26]. However, the synthetic methods of the pore-containing Si-based anode materials which have been reported are complicated, costly and difficult to scale up.

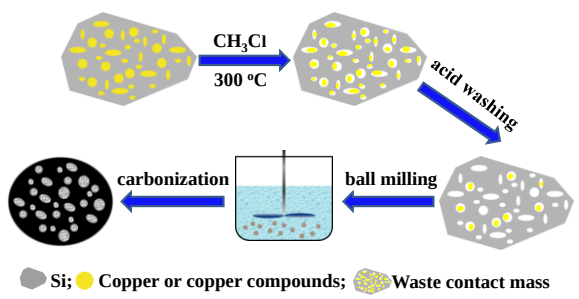

Fig. 1. Schematic illustration for the generating process of the waste contact mass and the preparation procedures for the pore-containing silicon/nitrogen-rich carbon composites.

Herein, we report the pore-containing silicon materials which are obtained from the waste contact mass of organosilane industry. Methylchlorosilanes are synthetized by the reaction of Si powder with chloromethane via copper or copper compounds as catalysts. The reaction occurs as below:

$$Si + CH_3Cl \xrightarrow{catalysts} SiR_{4-n}Cl_n (n = 1-4)$$

During this process, the industrial metallurgical-grade Si powder and the Cu-based catalyst particles are well mixed to form a contact mass. Then the contact mass reacts with CH_3Cl to produce methylchlorosilanes, and meanwhile, generates a large amount of waste contact mass due to the limitations of reaction kinetics and thermodynamics (Fig. 1). The waste contact mass consists of some metal, metal compounds, deposited carbon and 75-90 wt% of Si powder which has not been reacted. Ordinarily, the catalysts copper or copper compounds are recyled after a series of treatments, but the residual waste contact mass has not been utilized valuably. The underused waste contact mass contaminates the environment and takes up a lot of space to store. In this work, we use the residuals as raw materials to synthesize pore-containing Si/C composites as anode materials for lithium-ion batteries by simply dispersing the as-prepared pore-containing silicon from the waste contact mass into the nitrogen-rich carbon matrix derived from gelatin. The gelatin is adopted since it is cheap, environmentally friendly and commercially available. Moreover, the nitrogen atoms exist in the carbon material derived from gelatin in the form of pyridinic nitrogen, pyrrolic nitrogen, pyridonic nitrogen and graphitic nitrogen and it is believed that the nitrogen-rich carbon material plays a positive role for lithium insertion due to the stronger interaction between the nitrogen-rich carbon material and lithium[27,28]. In this paper, we analyze the morphology and structure of the waste contact mass comprehensively and thoroughly and further fabricate the pore-containing silicon/nitrogen-rich carbon composite with satisfactory cycling stability and rate capability through a very simple method. Obviously, this work exhibits a facile, low cost and eco-friendly way of taking full advantage of the waste contact mass from organosilane industry as a raw material for the fabrication of Si/C anode materials for lithium-ion batteries.

Experimental

Sample preparation

The waste contact mass of organosilane industry was provided by Jiangsu Taizhou Meilan Chemical Co., Ltd. Fig. 1 gives an overview of the synthesis process of the pore-containing silicon/nitrogen-rich carbon composites, named as WP-Si/C. Firstly, the waste contact mass was treated with sulfuric acid solution to remove the copper compounds and some metal impurities such as Al, Ca and Fe. Then the purified pore-containing silicon (WP-Si) particles were obtained. A small amount of copper may be left to enhance the electronic conductivity of the material. After milled with planetary ball mill, the WP-Si particles were dispersed in a 12% (wt/wt) gelatin aqueous solution by mechanical stirring for 4 h at 60 ^oC to insure a homogeneous distribution of the WP-Si particles in the gelatin matrix. The mixture was then carbonized at 800 ^oC in nitrogen (99.999%) for 3 h at a heating rate of 5 ^oC min^{-1} to obtain the WP-Si/C composites. Based on the weight ratios of the WP-Si particles and gelatin (1:2, 1:4 and 1:6), the as-prepared WP-Si/C composites were named as WP-Si/C-2, WP-Si/C-4 and WP-Si/C-6 accordingly. As a comparison, gelatin was also carbonized under the same experimental conditions and the obtained carbon was called GC.

Structural characterization

The contents of Si and other metal impurities in the waste contact mass before and after acid-washing treatment were determined quantitatively by inductively coupled plasma atomic emission spectrometer (ICP-AES, HORIBA Jobin Yvon ULTIMA-C). The microstructures of the samples were examined by scanning electron microscopy (SEM) (JSM-5600LV, JEOL, Tokyo, Japan) and transmission electron microscopy (TEM) (JEM-2010F, JEOL, Tokyo, Japan). Nitrogen adsorption-desorption isotherms of the composites were measured at 77 K with a NOVA1200 instrument (Quantachrome Corporation). Total specific area was determined by multipoint Braunauer-Emmett-Teller method. The BJH pore size distribution was calculated based on the desorption branch of the isotherm. The amount of carbon in the composites was determined by thermogravimetric (TG) analysis using a Perkin-Elmer TGA 7 thermogravimetric analyzer from 40 ^oC to 1000 ^oC with a heating rate of 10 ^oC min^{-1} in air. The phase composition of WP-Si, WP-Si/C composites and GC were determined by a Rikagu B/max-2400X with Cu Kα radiation in the 2θ range of 10^o to 90^o. Raman spectroscopy (Renishaw in Viamicro-Raman spectroscopy system equipped with a 514.5 nm laser) was used to investigate the existence of carbon of the WP-Si/C composites. X-ray photoelectron spectra (XPS) were recorded on an AXIS Ultra DLD spectrometer (Kratos) to characterize the surface composition.

Electrochemical measurements

Electrochemical experiments were performed using CR2025-type coin cells assembled in an argon-filled glove box with Celgard 2400 membrane as separator and lithium-foil as counter electrode. The electrolyte employed was 1 M $LiPF_6$ in the mixture of ethylene carbonate (EC) and dimethyl carbonate (DMC) (1:1 in volume ratio). The working electrode was prepared by casting a mixture of 60 wt% active material, 20 wt% acetylene black and 20 wt% sodium alginate dissolved in deionized water on a copper current collector. The active materials mass loading was approximately 1 mg cm^{-2}. Prior to cell fabrication, the electrodes were degassed in vacuum oven at 120 ^oC for at least 6 h. The electrochemical performances were evaluated on a LAND CT2001A multi-channel battery test system at room temperature. If not mentioned otherwise, the galvanostatic voltage cutoffs were 0.01 and 1.5 V vs Li/Li^+. Cyclic voltammetry (CV) measurement was performed on a CHI660D electrochemical workstation at a scan rate of 0.1 mV s^{-1}. Electrochemical impedance spectroscopy (EIS) was also carried out on this instrument in the frequency range from 10^5 to 0.01 Hz and the amplitude of the used perturbation was 10 mV. The specific capacity was calculated based on the total mass of the active material.

Results and discussion

Table 1 shows the ICP-AES analytic results of the waste contact mass before and after acid-washing treatment. The waste contact mass itself has a high content of Si, about 82.3 wt%. The content of Al, Ca, Cu and Fe is 0.5 wt%, 0.4 wt%, 7.5 wt% and 1.4 wt%, respectively. The high content of Cu is from the copper-based catalysts which refer to copper or copper compounds during the production process of methylchlorosilanes. In addition to Si and these metal elements, it still contains a small amount of carbon formed during the synthetic process of the methylchlorosilanes and the combined oxygen to balance the metal ions in the waste contact mass. After the acid-washing treatment, the Si content can reach 98 wt%, much higher than that of the waste contact mass, suggesting its high purity. The remaining 0.4 wt% of copper in the elemental form is from the copper-based catalysts. It is believed that the presence of Cu may play a positive role in enhancing the electrical conductivity of the WP-Si/C materials[29].

Table 1 ICP-AES analytic results of the waste contact mass before (a) and after acid-washing treatment (b).

	Si /%	Al /%	Ca /%	Cu /%	Fe /%
a	82.3	0.5	0.4	7.5	1.4
b	98	<0.1	<0.1	0.4	<0.1

The morphology of WP-Si is shown in Fig. 2. It clearly shows that the WP-Si particles are in irregular shapes with the diameter about 20 μm or more. The surface of some particles is very smooth (the inset of Fig. 2a), whereas some other particles have the gap-shaped surface, which is very rough (the inset of Fig. 2b). During the process of the reaction between the contact mass and CH_3Cl, the surface of the metallurgical-grade Si particles is radially etched and consumed centering on the Cu-based catalyst particles and the pores are formed. The TEM image (Fig. 2c) shows the pore structure of the WP-Si, which is believed to be benificial to partially accommodate the huge volume change during the charge and discharge process. Its pore structure was further evaluated by specific surface area method which was conducted according to the nitrogen adsorption-desorption isotherms measurements (Fig. 3(a)). The specific surface area of the waste contact mass after acid washing of some of the catalyst particles which occupy the position of pores (WP-Si) is determined to be 20.2 $m^2 g^{-1}$ by the BET method, much higher than that before acid washing (6.1 $m^2 g^{-1}$). The pore size distribution determined by the BJH analysis (Fig. 3(b)) indicates that the pore diameter of the waste contact mass before and after acid-washing treatment lies in the size range of 1-2 nm and 10-100 nm. The TEM image under high magnification (Fig. 2d) shows the interplanar spacing of the WP-Si, which are consistent with the (111) planes of silicon. From the TEM, it can be seen that the WP-Si is coated with a thin layer of about 5 nm with amorphous microstructure which may refer to both the small amount of carbon from the synthetic process of the methylchlorosilanes and the SiO_2 layer formed during the acid-washing treatment. The carbon showing a relatively amorphous microstructure is beneficial to enhance the electrical conductivity of the material, although its content is very low.

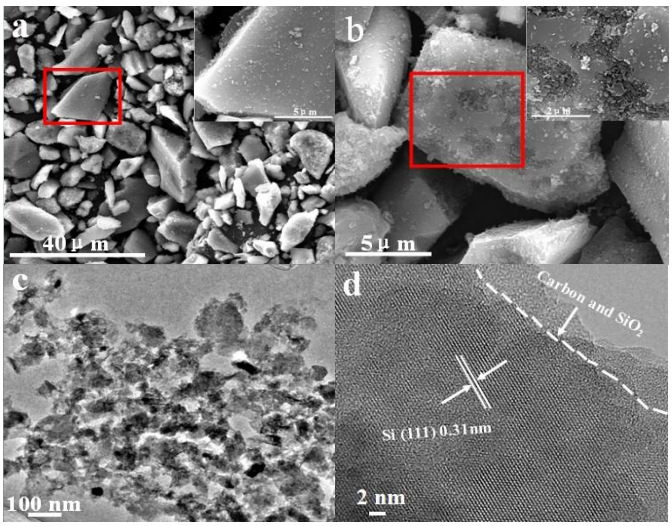

Fig. 2. SEM images (a and b), TEM image (c) and HR-TEM image (d) of WP-Si.

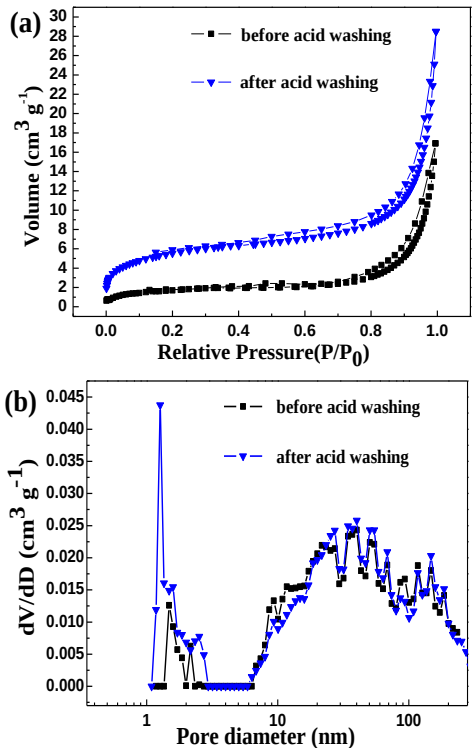

Fig. 3. (a) Nitrogen adsorption-desorption isotherms and (b) the pore size distribution of the waste contact mass before and after acid-washing treatment.

Fig. 4 presents the thermogravimetric (TG) analysis curves of GC and the WP-Si/C composites from 40 °C to 1000 °C in air. The weight losses occur in the temperature range of 400 °C to 700 °C for the WP-Si/C composites corresponding to the oxidation of the carbon. When the temperature is higher than 700 °C, the carbon is completely combusted. Therefore, the carbon contents in the WP-Si/C composites determined by the TG analysis are estimated to be 28 wt%, 38 wt% and 45 wt% for WP-Si/C-2, WP-Si/C-4 and WP-Si/C-6, respectively. A little weight increase at the temperature above 800 °C is ascribed to the oxidation of silicon into SiO_x in the WP-Si/C composites.

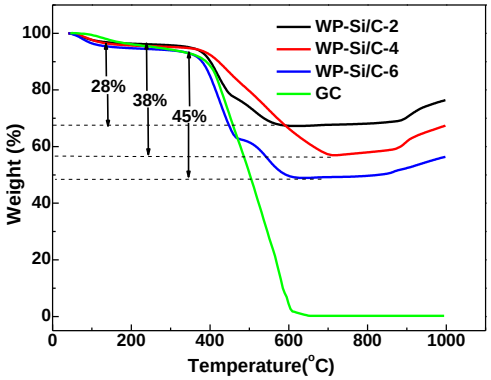

Fig. 4. TG curves of GC and the WP-Si/C composites under air atmosphere from 40 °C to 1000 °C.

The XRD patterns of the GC, WP-Si and WP-Si/C composites are shown in Fig. 5. For the XRD pattern of GC, two broad diffraction peaks are observed at 2θ of 23° and 43°, showing a non-graphitized structure[30]. For WP-Si and WP-Si/C composites, the intensive well-defined peaks at 2θ of 28.4°, 47.4°, 56.2°, 69.2°, 76.5° and 88.1° can be indexed as the (111), (220), (311), (400), (331) and (422) planes of Si crystals[26], respectively. After acid-washing treatment, all peaks of the WP-Si are solely assigned to Si, further indicating its high purity. Moreover, it can be noted that the peaks corresponding to the amorphous carbon derived from gelatin can not be detected obviously in the WP-Si/C composites, which is possibly due to the low content of GC in the WP-Si/C composites compared with the WP-Si.

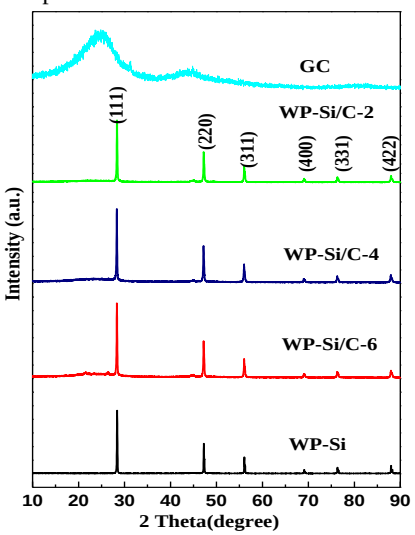

Fig. 5. XRD patterns of GC, WP-Si and WP-Si/C composites.

The Raman spectra of the WP-Si and WP-Si/C composites are shown in Fig. 6. The strong intense peak of the WP-Si at 515 cm^{-1} corresponds to the crystalline Si[31]. After dispersed in the carbon matrix, the silicon peak shifts to around 520 cm^{-1}, which is probably because of a phonon confinement effect or a masking effect[32]. Another two peaks at around 1350 cm^{-1} and 1596 cm^{-1} of the WP-Si/C composites are assigned to the disordered carbon (D band) and the graphitic carbon (G band), respectively[25,33]. These results confirm the presence of the carbon matrix in the WP-Si/C composites. In addition, the relative intensity between carbon and the WP-Si has changed observably, which may be because of the increase of the gelatin content leading to more carbon coating on the surface of the WP-Si.

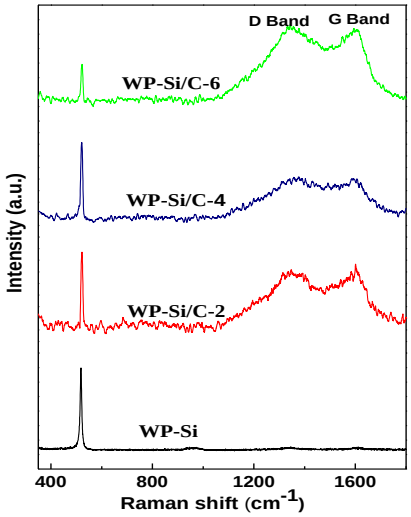

Fig. 6. Raman spectra of the WP-Si and WP-Si/C composites.

Fig. 7 presents the XPS spectra of WP-Si and WP-Si/C-4. The wide scan XPS spectra of Fig. 7(a) reveal the composition of the exterior surface of WP-Si and WP-Si/C-4. The XPS analysis shows major peaks which are due to silicon (Si 2p), nitrogen (N 1s), oxygen (O 1s) and carbon (C 1s). All of the peaks are classified according to their binding energy. The Si 2p spectrum for WP-Si in Fig. 7(b) shows a strong peak for SiO_2 at 102.5 eV and a weak peak for Si-Si at 98.3 eV[34]. The presence of SiO_2 is due to the native oxide formation during the synthetic process of the methylchlorosilanes. However, for WP-Si/C-4, as the WP-Si particles are well covered by the carbon derived from gelatin, there is only a weaker peak shown at 100.4 eV for SiO_2, without the detection of the Si-Si signal. Fig. 7(c) compares the N 1s spectra of the two samples. By contrast with WP-Si, the N 1s spectrum of WP-Si/C-4 shows strong peaks at 395.3 eV and 397.3 eV, indicating that the carbon matrix of GC is rich in nitrogen. And dispersing the WP-Si particles in the nitrogen-rich carbon is believed to be beneficial for lithium insertion[35,36]. The O 1s spectrum in Fig. 7(d) shows a strong O 1s peak for WP-Si, implying the presence of SiO_2, consistent with the Si 2p spectrum for WP-Si. For WP-Si/C-4, a relatively weak O 1s peak is observed, further demonstrating that the WP-Si particles are well covered by the carbon rich in nitrogen. Fig. 7(e) presents the C 1s spectra of the both samples. For WP-Si, the peak of C 1s at 284.1 eV may be due to the presence of carbon deposit formed during synthetic process of the methylchlorosilanes. Whereas, for WP-Si/C-4, the peak of C 1s at 281.6 eV may arise from the carbon pyrolysed from gelatin, indicating the formation of nitrogen-rich carbon layer on the WP-Si particles.

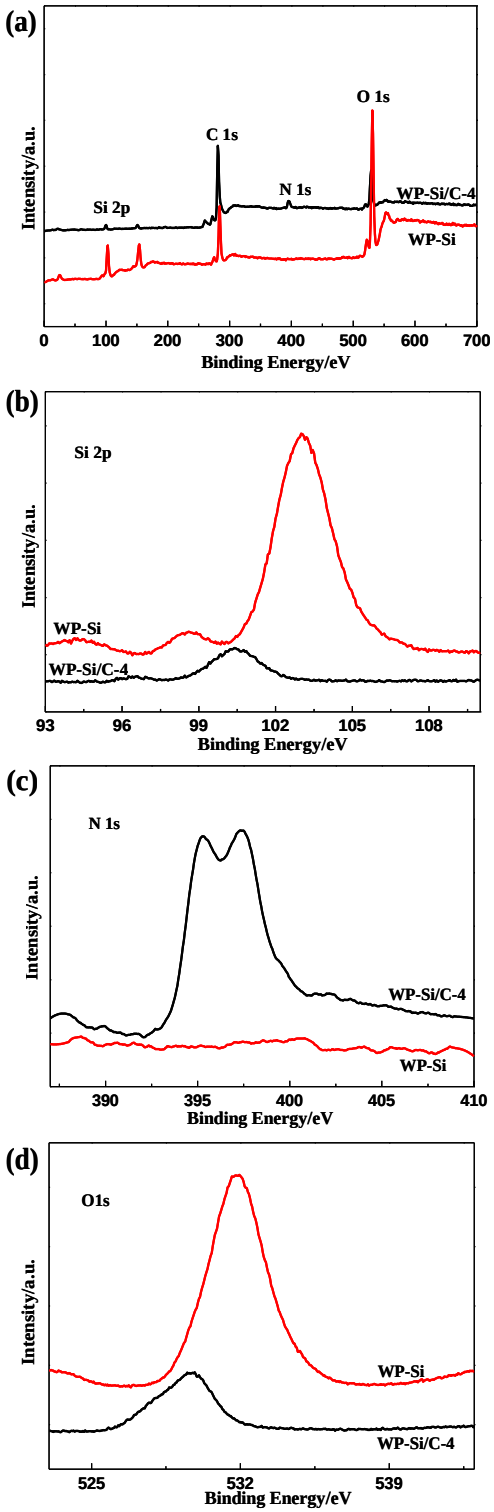

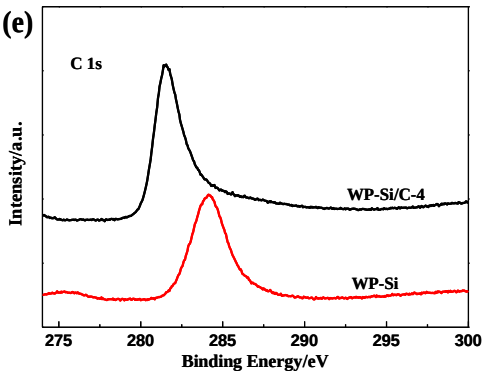

Fig. 7. XPS spectra of WP-Si and WP-Si/C-4
(a) wide spectra; (b) Si 2p ; (c) N 1s ; (d) O 1s ; (e) C 1s.

The morphology of the as-prepared WP-Si/C-4 composite is characterized by SEM and TEM. After ball-milling, the size of the WP-Si is less than 5 μm, beneficial for the improvement of the cycling performance. From Fig. 8a, it can be seen that the WP-Si particles distribute uniformly in the carbon matrix. In TEM image (Fig. 8b), it is evident that the WP-Si particles are completely covered by carbon layer. The high resolution TEM image (Fig. 8c) shows the interplanar spacing of the WP-Si, which are consistent with the (111) planes of silicon. Besides, it can be seen that the WP-Si is covered with a compact carbon layer with the amorphous microstructure, further corroborating that the WP-Si particles disperse homogeneously in the nitrogen-rich carbon matrix. The pore structure of the WP-Si is confirmed with TEM image (Fig. 2c) and its specific surface area. Based on the above results, the carbon matrix in the composite and the pores within the WP-Si particles are expected to accommodate the large volume change during the cycling effectively.

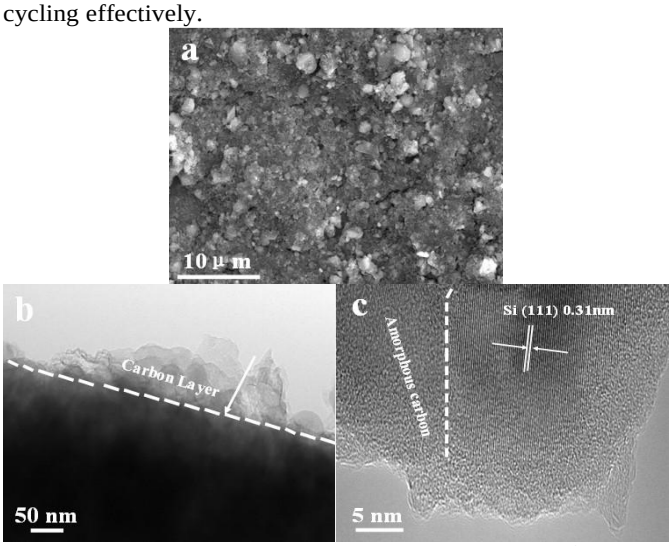

Fig. 8. SEM image (a), TEM image (b) and HR-TEM image (c) of the WP-Si/C-4.

Fig. 9 exhibits the CV curves in the initial three cycles of WP-Si/C-4 electrode at the scan rate of 0.1 mV s^{-1}. In the first cathodic scanning cycle, the reduction peak located at around 0.6 V may be ascribe to the formation of the SEI film[25], which disappears from the second cycle. The peak at 0.01 V corresponds to the Li-insertion process of crystalline Si to form the amorphous Li_xSi phase. What's more, an additional peak at about 0.2 V appears from the second cathodic scan. In the

anodic scanning cycle, two peaks located at 0.3 V and 0.5 V become gradually broader and stronger, which are attributed to the phase transition between amorphous Li_xSi and amorphous silicon. After the first cycle, the scans show a repeatable shape. The CV curve area is increasing in the subsequent cycles, which is due to the initial activation of the electrode material, enabling more Li to alloy with Si[11,37,38].

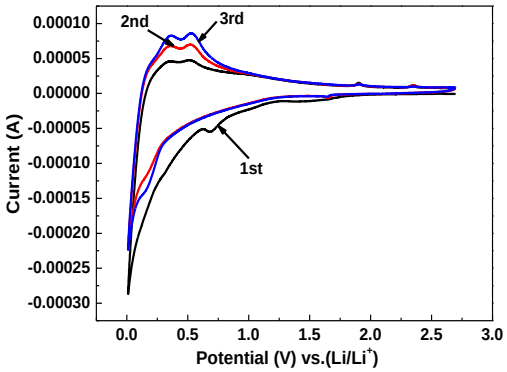

Fig. 9. Cyclic voltammogram curves of the WP-Si/C-4 electrode from the first cycle to the third cycle at a scan rate of 0.1 mV s^{-1}.

The as-synthesized GC, WP-Si and WP-Si/C composites are employed as electrode materials to assemble laboratory lithium-ion cells. Fig. 10a shows the discharge and charge curves of the GC, WP-Si and WP-Si/C composites during the first cycle in the voltage window of 0.01-1.5 V at a current density of 100 mA g^{-1}. The discharge and charge curves of WP-Si and WP-Si/C composites exhibit the same shape, displaying a long flat plateau below 0.1 V during the first cycle discharge and a voltage plateau at 0.45 V during the first cycle charge. Moreover, it can be seen that WP-Si shows the initial discharge and charge capacity of 2746 and 2123 mA h g^{-1} with a coulombic efficiency of 77%. While GC delivers a poor initial discharge capacity of 788 mA h g^{-1} and charge capacity of 262 mA h g^{-1}, with a coulombic efficiency of 33%. As a comparison, WP-Si/C-6, WP-Si/C-4 and WP-Si/C-2 show first cycle discharge capacity of 1083, 1143 and 1844 mA h g^{-1} and first cycle charge capacity of 630, 932 and 1448 mA h g^{-1}, with the initial coulombic efficiencies of 58%, 82% and 79%, respectively. The large irreversible capacity losses between the discharge and charge in the first cycle of WP-Si should originate from the dead Li which was not dealloyed during the discharge process because of pulverization of the electrode from the huge volume change and the solid-electrolyte interface (SEI) layer formation on the surface of the electrode. The low initial coulombic efficiency of GC material is because of the consumption of Li during the formation process of SEI film on the surface of the GC electrode and the irreversible lithium intercalation due to the residual electrochemically active surface groups such as C-H in the low-temperature pyrolyzed carbon materials[30]. The huge initial irreversible capacity of the WP-Si/C composites may be mainly attributed to the reasons mentioned above. What's more, the initial coulombic efficiency has a tendency to increase as the carbon content of the WP-Si/C composite decreases.

Fig. 10b demonstrates the cycling performance of the as-prepared GC, WP-Si and WP-Si/C composites at a current density of 100 mA g^{-1}. Although the capacity of the bare WP-Si is much higher than that of the WP-Si/C composites in the first cycle due to the presence of low-capacity carbon in the latter, the capacity of the bare WP-Si drops quickly to only about 95 mA h g^{-1} after 100 cycles. The reason for the rapid capacity loss is that the pore structure of the WP-Si is not rich enough to effectively suppress the pulverization of silicon during lithium insertion/extraction processes and also the continual formation of very thick SEI film on the surface of the particles. For comparison, the bare carbon derived from gelatin shows a stable but very low capacity of 253 mA h g^{-1} after 100 cycles. Apparently, after dispersing the WP-Si particles into the nitrogen-rich carbon matrix, the electrochemical performance of the as-prepared WP-Si/C composites has been improved a lot. It can be seen that during the first 50 cycles, the WP-Si/C-2 composite shows the highest specific capacity because of its high Si content. However, its capacity drops very quickly to 513 mA h g^{-1} after 100 cycles with the capacity retention of only 36% against at the second cycle. WP-Si/C-6 exhibits a much better cycling performance than WP-Si/C-2 with the capacity retention of about 65% against at the second cycle after 100 cycles. But it delivers a relatively low reversible capacity of 443 mA h g^{-1} because of the higher GC content. Therefore, in the WP-Si/C composites, more WP-Si contributes to higher specific capacity and more GC to better cycle stability. In order to get the sample with the best electrochemical performance, the WP-Si/C composite should have the optimal WP-Si and GC ratio. Compared with the two samples mentioned above, WP-Si/C-4 which contains 62 wt% WP-Si and 38 wt% GC delivers the highest reversible capacity of 748 mA h g^{-1} and excellent cycle stability with capacity retention of 70% against at the second cycle after 100 cycles. From the above results, it can come to the conclusion that the GC plays a very important role in the WP-Si/C composites. It not only serves as a cushion to buffer the large volume change of WP-Si during the Li-ion insertion/extraction but also provides more pathways for the electron transportation and ultimately enhance the electrical conductivity of the material. Fig. 10c shows the rate performance of the WP-Si/C-4 composite at different current densities. It delivers reversible capacities of 776, 642, 522 and 457 mA h g^{-1} at a current density of 100, 200, 400 and 600 mA g^{-1}, respectively, showing a good rate performance. It is believed that the good cycling stability and rate performance of the WP-Si/C-4 composite benefit from both the pore structure of the WP-Si particles and the nitrogen-rich carbon matrix with high electrical conductivity.

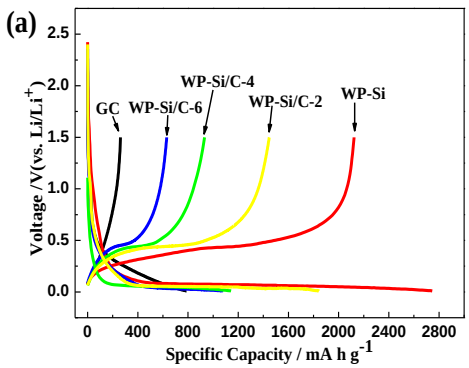

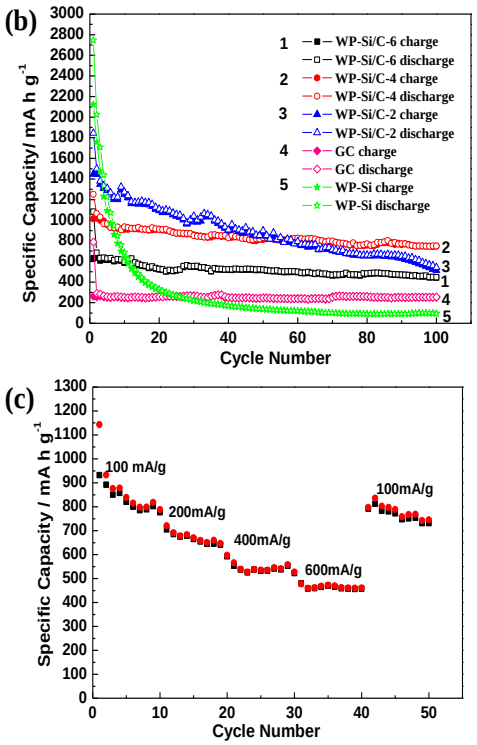

Fig. 10. (a) The first cycle charge-discharge curves of GC, WP-Si and WP-Si/C composites at 100 mA g^{-1} in the voltage window of 0.01-1.5 V; (b) The cycling performance of GC, WP-Si and WP-Si/C composites at 100 mA g^{-1}; (c) The rate performance of WP-Si/C-4 at various current densities.

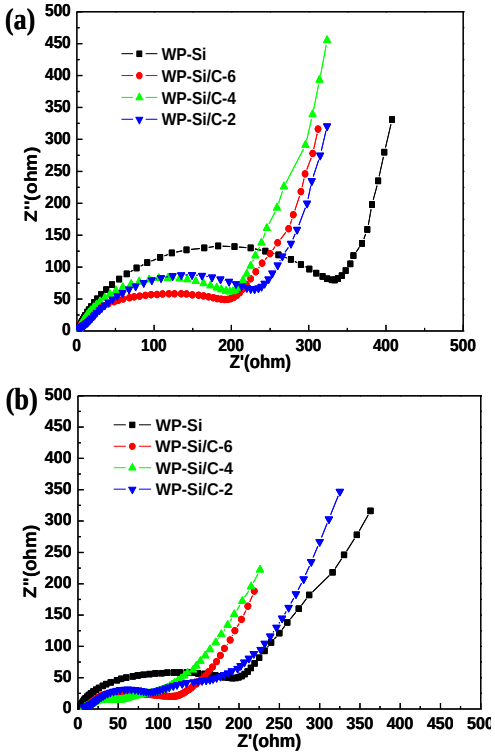

Fig. 11. Nyquist plots of the WP-Si and WP-Si/C composites: (a) before cycling and (b) after 100 cycles.

To further understand the mechanism of the capacity degradation of the WP-Si and WP-Si/C composites, EIS was recorded from 10^5 to 0.01 Hz before cycling and after 100 cycles. As shown in Fig. 11, all of them show an inclined low-frequency line with angle more than 45°, which is assigned to the lithium diffusion impedance. The electrodes of the WP-Si and WP-Si/C composites show only one semicircle representing the charge transfer resistance (R_{ct}) of Li-ion insertion, while they show two semicircles after 100 cycles. The first semicircle is associated with the resistance of the SEI film (R_f) and the second semicircle is assigned to the charge-transfer resistance of Li-ion insertion[39,40]. According to the Nyquist plots before cycling (Fig. 11(a)), the charge transfer resistance of WP-Si/C composites are much lower than that of WP-Si which indicates that the WP-Si/C composites have higher electric conductivity than the bare WP-Si electrode and the carbon matrix supplies fast charge-transfer network on the interface of WP-Si and electrolyte. After 100 cycles (Fig. 11(b)), the electrodes of the WP-Si and WP-Si/C composites show the decreased values of R_{ct} by comparison with that before cycling, which may be attributed to the activation of the electrodes and the more sufficiently contact between the activated materials and the electrolyte. Moreover, compared with the WP-Si electrode, the smaller R_{ct} of the WP-Si/C electrodes mean a smaller electrochemical reaction resistance during the lithiation/delithiation process and the smaller R_f means a stable SEI film formed after carbon coating, which decreases the resistance for Li^+ migration through the surface film[24]. What's more, the WP-Si/C-4 electrode has the smallest values of R_f and R_{ct} which is in good agreement with the above reported good electrochemical performance.

Conclusions

In summary, the pore-containing silicon/nitrogen-rich carbon materials have been successfully fabricated by using the waste contact mass of organosilane industry as the pore-containing silicon source and gelatin as the nitrogen-rich carbon precursor via acid washing, mechanical stirring and a subsequent pyrolysis process. It is found that the capacity and cycling stability of the pore-containing silicon/nitrogen-rich carbon materials are related to the proportion of the pore-containing silicon and nitrogen-rich carbon. When the ratio between the gelatin and pore-containing silicon from the waste contact mass is four to one, the obtained pore-containing silicon/nitrogen-rich carbon materials contains 62 wt% pore-containing silicon and 38 wt% nitrogen-rich carbon, showing the best electrochemical performance with a reversible capacity of 748 mA h g^{-1} after 100 cycles at a current density of 100 mA g^{-1} and 457 mA h g^{-1} at 600 mA g^{-1}, much higher than those of commercial graphite anodes. The superior electrochemical performance is attributed to the pore structure within the pore-containing silicon particles to absorb the large volume expansions and the nitrogen-rich carbon matrix which can accommodate the volume change as well as improve the electronic conductivity. These results of the present study demonstrate the potential possibility of making full use of the waste contact mass of organosilane industry as a promising raw material for Si/C anode materials through low cost and environmental friendly method.

Acknowledgements

This work was financially supported by the Fund from National High Technology Research and Development Program 863 (no. 2011AA11A256, no. 2012AA052202).

Notes and references

[a] School of Chemical Engineering and Environment, Beijing Institute of Technology, Beijing 100081, China. E-mail: lulus1987@163.com;
[b] Military Power Sources Research and Development Center, Research Institute of Chemical Defense, Beijing 100191, China. Fax: +86-10-66748499; Tel: +86-10-66705840; E-mail: wangweikun2002@163.com; wab_wang2000@aliyun.com

References

1 J. B. Goodenough and Y. Kim, Chem. Mater., 2010, **22**, 587.
2 M. Armand and J. M. Tarascon, Nature, 2008, **451**, 652.
3 M. Winter, J.O. Besenhard, M.E. Spahr and P. Novak, Adv. Mater., 1998, **10**, 725.
4 N. Liu, H. Wu, Matthew T. McDowell, Y. Yao, C. M. Wang and Y. Cui, Nano Lett., 2012, **12**, 3315.
5 X. H. Liu, L. Zhong, S. Huang, S.X. Mao, T. Zhu and J.Y. Huang, ACS Nano, 2012, **6**, 1522.
6 T. Zhang, J. Gao, L. J. Fu, L. C.Yang, Y. P. Wu and H. Q. Wu, J. Mater. Chem., 2007, **17**, 1321.
7 Y. Liu, X. Qiu and X. Guo, J. Mater. Chem. A, 2013, **1**, 14075.
8 C. Martin, M. Alias, F. Christien, O. Crosnier, D. Bélanger and T. Brousse, Adv. Mater., 2009, **21**, 4735.
9 R. Yi, J. Zai, F. Dai, M. L. Gordin and D.Wang, Electrochem. Commun., 2013, **36**, 29.
10 Ⅱ-seok Kim, P. N. Kumta and G. E. Blomgren, Electrochem. Solid State Lett., 2000, **3**, 493.
11 C. K. Chan, H. Peng, G. Liu, K. Mcllwrath, X. F. Zhang, R. A. Huggins and Y. Cui, Nat. Nanotechnol., 2008, **3**, 31.
12 L. H. Lin, X. Z. Sun, R. Tao, Z. C. Li, J. Y. Feng and Z. J. Zhang, J.Appl. Phys., 2011, **110**, 7.
13 L. Cui, Y. Yang, C. Hsu and Y. Cui, Nano. Lett., 2009, **9**, 3370.
14 L. F. Cui, L. B. Hu, J. W. Choi and Y. Cui, ACS Nano, 2010, **4**, 3671.
15 M. H. Park, M. G. Kim, J. Joo, K. Kim, S. Ahn, Y. Cui and J. Chao, Nano Lett., 2009, **9**, 689.
16 H. Wu, G. Chan, J. W. Choi, I. Ryu, Y. Yao, M. T. McDowell, S. W. Lee, A. Jackson, Y. Yang, L. Hu and Y. Cui, Nat. Nanotechnol., 2012, **7**, 310.
17 Y. Yao, M.T. McDowell, I. Ryu, H. Wu, N. Liu, L. B. Hu, W. D. Nix, and Y. Cui, Nano Lett., 2011, **11**, 2949.
18 P. R. Abel, Y. M. Lin, H. Celio, A. Heller and C. B. Mullins, ACS Nano, 2012, **6**, 2506.
19 M. K. Datta, J. Maranchi, S. J. Chung, R. Epur, K. Kadakia, P. Jampani and P. N. Kumta, Electrochim. Acta, 2011, **56**, 4717.
20 H. Kim, B. Han, J. Choo and J. Cho, Angew. Chem., Int. Ed., 2008, **47**, 10151.
21 H. P. Jia, P. F. Guo, J. Yang, J. L. Wang, Y. N. Nuli and Z. Yang, Adv. Energy Mater., 2011, **1**, 1036.
22 Y. Zhao, X. Z. Liu, H. Q. Li, T. Y. Zhai and H. S. Zhou, Chem. Commun., 2012, **48**, 5079.
23 M. Thakur, R. B. Pernites, N. Nitta, M. Isaacson, S.L. Sinsabaugh, M. S. Wong and S. L. Biswal, Chem. Mater., 2012, **24**, 2998.
24 M. S. Wang and L. Z. Fan, J. Power Sources, 2013, **244**, 570.
25 J. C. Guo, X. L. Chen and C. S. Wang, J. Mater. Chem., 2010, **20**, 5035.
26 H. Tao, Li. Fan and X. Qu, Electrochimica Acta, 2012, **71**, 194.
27 Y. Mao, H. Duan, B. Xu, L. Zhang, Y. S. H, C. C. Zhao, Z. X. Wang, L. Q. Chen and Y. S. Yang, Energy Environ. Sci., 2012, **5**, 7950.
28 L. Qie, W. M. Chen, Z. H. Wang, Q. G. Shao, X. Li, L. X. Yuan, X. L. Hu, W. X. Zhang and Y. H. Huang, Adv. Mater., 2012, **24**, 2047.
29 J. W. Kim, J. H. Ryu, K. T. Lee and S. M. Oh, J. Power Sources, 2005, **147**, 227.
30 B. Xu, L. Shi, X. W. Guo, L. Peng, Z. X. Wang, S. Chen and G. P. Cao, Electrochimica Acta, 2011, **56**, 6464.
31 L. Guo, W.Yoon and B. Kim, Electron Mater. Lett., 2012, **8**, 405.
32 C. Meier, S. Lüttjohann, V.G.Kravets, H. Nienhaus, A.Lorke, and H.WIGGERS, Phys. E: Low-dimensional Syst.Nanostructu., 2006, **32**, 155.
33 J. T. McCann, B. Lim, R. Ostermann, M. Rycenga, M. Marquez and Y. Xia, Nano Lett., 2007, **7**, 2470.
34 J. H. Noh, K. Y. Lee and J. K. Lee, Trans. Nonferrous Met. Soc. China, 2009, **19**, 1018.
35 Y. P. Wu, S. B. Fang and Y. Y. Jiang, Solid State Ionics, 1999, **120**, 117.
36 Y. P. Wu, C. Y. Jiang, C. R. Wan, S. B. Fang and Y. Y. Jiang, J. Appl. Polym. Sci., 2000, **77**, 1735.
37 M. Ge, J. Rong, X. Fang and C. Zhou, Nano Lett., 2012, **12**, 2318.
38 M. Green, E. Fielder, B. Scrosati, M. Wachtler and J. S. Moreno, Electrochem. Solid-State Lett., 2003, **6**, A75-A79.
39 C. S. Wang, A. J. Appleby and F. E. Little, Electrochimica Acta, 2001, **46**, 1793.
40 R. Ruffo, S. Hong, C. K. Chan, R. A. Huggins and Y. Cui, J. Phys. Chem., 2009, **113**, 11390.

A graphical and textual abstract

The scalable pore-containing silicon/nitrogen-rich carbon materials are fabricated by using the waste contact mass of organosilane industry as silicon source.